*Multiscale Analysis of Complex Time Series: Integration of Chaos and Random Fractal Theory, and Beyond*
by Jianbo Gao, Yinhe Cao, Wen-wen Tung and Jing Hu


## CHAPTER 4

# FOURIER ANALYSIS AND WAVELET MULTIRESOLUTION ANALYSIS

In electrical engineering, frequency analysis of signals and systems is a central topic of signal processing. When used intelligently, Fourier analysis can be very revealing, even though the signals to be analyzed are very complicated. Unfortunately, even after several courses on signal processing, many electrical engineering graduate students still feel paralyzed when asked to analyze real data. We suspect that this problem may be even more acute among nonelectrical engineers. To help readers get started, especially those less experienced in data analysis, we devote Sec. 4.1 to a brief discussion of Fourier analysis, with emphasis on analysis of real data. We hope that after this treatment, readers will find complicated signals to be more friendly. Some of the examples discussed in Sec. 4.1 also illustrate fractal signals. In Sec. 4.2, we describe wavelet multiresolution analysis (MRA). In later chapters, wavelet MRA will be extensively used to estimate key parameters of random fractal processes. In order to focus on big pictures and to proceed quickly to later chapters, derivations of some key equations described below are omitted. They can be found in the Bibliographic Notes at the end of the chapter.

## 4.1 FOURIER ANALYSIS

### 4.1.1 Continuous-time (CT) signals

Suppose we are given a periodic signal $x(t)$ with period $T_p$. It can be represented as a linear combination of harmonically related complex exponentials of the form

$$x(t) = \sum_{k=-\infty}^{\infty} c_k e^{j2\pi k F_0 t}, \tag{4.1}$$

where $F_0 = 1/T_p$ and $j^2 \equiv -1$. This is called Fourier series representation of periodic signals. One can think of the exponential signals

$$\{e^{j2\pi k F_0 t}, \quad k = 0, \pm 1, \pm 2, \cdots\}$$

as the basic building blocks. These building blocks are orthogonal, i.e.,

$$\int_{t_0}^{t_0+T_p} e^{j2\pi k F_0 t} e^{-j2\pi l F_0 t} dt = \begin{cases} 0, & k \neq l \\ T_p, & k = l, \end{cases}$$

where $t_0$ is arbitrary. Therefore, the coefficient $c_k$ is given by

$$c_k = \frac{1}{T_p} \int_{T_p} x(t) e^{-j2\pi k F_0 t} dt, \tag{4.2}$$

where integration is carried out over any interval of length $T_p$. In general, $c_k$ is complex valued. It can be written as

$$c_k = |c_k| e^{j\theta_k}.$$

Graphically, one can plot $|c_k|$ and/or $\theta_k$ against the frequency $kF_0$. Such plots are called line spectra with equidistant lines. The line spacing is equal to the fundamental frequency, which in turn is the inverse of the fundamental period of the signal.

Now let us allow the period to increase without limit. The line spacing then tends toward zero. In the limit, when the period becomes infinite, the signal becomes aperiodic and its spectrum becomes continuous. Guided by this argument, and replacing summation by integration, one readily obtains the following Fourier transform of aperiodic signals:

$$x(t) = \int_{-\infty}^{\infty} X(F) e^{j2\pi F t} dF. \tag{4.3}$$

The coefficient $X(F)$ is given by

$$X(F) = \int_{-\infty}^{\infty} x(t) e^{-j2\pi F t} dt. \tag{4.4}$$

Comparing Eq. (4.4) with Eq. (4.2), we find that

$$T_p c_k = X(kF_0) = X\left(\frac{k}{T_p}\right).$$

Thus the Fourier coefficients are samples of $X(F)$ taken at multiples of $F_0$ and scaled by $F_0$ (multiplied by $1/T_P$). In other words, the spectrum of an aperiodic signal is the envelope of the line spectrum in the corresponding periodic signal obtained by repeating the aperiodic signal with period $T_p$.

Like $c_k$, $X(F)$ is complex valued. Its magnitude square,

$$S_{xx}(F) = |X(F)|^2,$$

is called the energy density spectrum. Parsavel's theorem states that

$$E_x = \int_{-\infty}^{\infty} |x(t)|^2 dt = \int_{-\infty}^{\infty} |X(F)|^2 dF.$$

### 4.1.2 Discrete-time (DT) signals

We start from a periodic sequence $x(n)$ with period $N$, that is, $x(n+N) = x(n)$ for all $n$. The Fourier series representation for $x(n)$ consists of $N$ harmonically related exponential functions

$$e^{j2\pi kn/N}, \qquad k = 0, 1, \cdots, N-1$$

and is expressed as

$$x(n) = \sum_{k=0}^{N-1} c_k e^{j2\pi kn/N}. \tag{4.5}$$

The orthogonality of the basis functions for the CT case is now replaced by the following formula:

$$\sum_{k=0}^{N-1} e^{j2\pi kn/N} = \begin{cases} N, & k = 0, \pm N, \pm 2N, \cdots \\ 0 & \text{otherwise.} \end{cases}$$

With this equation, one can readily find

$$c_k = \frac{1}{N} \sum_{n=0}^{N-1} x(n) e^{-j2\pi kn/N}. \tag{4.6}$$

It is easy to see that $\{c_k\}$ is also periodic with period $N$. The sequence $|c_k|^2$, $k = 0, 1, \cdots, N-1$ is the distribution of power as a function of frequency and is called the power density spectrum (or power spectral density (PSD)). Parsavel's relation now becomes

$$P_x = \sum_{k=0}^{N-1} |c_k|^2 = \frac{1}{N} \sum_{n=0}^{N-1} |x(n)|^2. \tag{4.7}$$

Next, we discuss the Fourier transform of a finite-energy, aperiodic DT signal $x(n)$. It is defined as

$$X(\omega) = \sum_{n=-\infty}^{\infty} x(n)e^{-j\omega n}. \tag{4.8}$$

Physically, $X(\omega)$ represents the frequency content of the signal $x(n)$. One can readily prove that $X(\omega)$ is periodic with period $2\pi$, that is,

$$X(\omega + 2\pi k) = X(\omega), \qquad k = \pm 1, \ \pm 2, \ \cdots .$$

This property indicates that the frequency range for any DT signal is limited to $(-\pi, \pi)$, or equivalently, $(0, 2\pi)$. In contrast, the frequency range for a CT signal is $(-\infty, \infty)$. When Eq. (4.8) is expressed in terms of frequency $f$, where $\omega = 2\pi f$, we have

$$X(f) = \sum_{n=-\infty}^{\infty} x(n)e^{-j2\pi fn}. \tag{4.9}$$

Since $X(\omega)$ is periodic with period $2\pi$, $X(f)$ is periodic with period 1.

We now derive the inverse transform. Using the following orthogonality condition

$$\int_{-\pi}^{\pi} e^{i\omega(m-n)}d\omega = \begin{cases} 2\pi, & m = n \\ 0, & m \neq n \end{cases}$$

under suitable convergence conditions, we multiply both sides of Eq. (4.8) by $e^{j\omega n}$ and integrate; then we have

$$x(n) = \frac{1}{2\pi}\int_{2\pi} X(\omega)e^{j\omega n}d\omega. \tag{4.10}$$

The energy of a DT signal $x(n)$ can be defined as

$$E_X = \sum_{n=-\infty}^{\infty} |x(n)|^2.$$

It also can be expressed as integration of $X(\omega)$, yielding the following Parsavel's relation for DT aperiodic signals with finite energy:

$$E_X = \sum_{n=-\infty}^{\infty} |x(n)|^2 = \frac{1}{2\pi}\int_{2\pi} |X(\omega)|^2 d\omega \ < \ \infty.$$

As in CT aperiodic signals

$$S_{xx}(\omega) = |X(\omega)|^2$$

is called the energy density spectrum of $x(n)$. In Sec. 3.3.1, we defined the autocorrelation function of a stochastic process. Let $R_{xx}(m)$ denote the autocorrelation function of $x(n)$. We have the following famous theorem.

**Wiener-Khintchine theorem**: $R_{xx}(m)$ and $S_{xx}$ form a Fourier transformation pair.

Instead of proving this theorem, we illustrate it with an example.

**Example 1**: In Sec. 3.3.2, we discussed an AR(1) process, defined by

$$x_{n+1} = ax_n + \eta_n, \tag{4.11}$$

where, for simplicity, we took the mean $\overline{x}$ of the process to be zero (as will be discussed shortly, the mean contributes to a DC component in the Fourier transform). The autocorrelation function of the AR(1) process is given by

$$R_{xx}(m) = \frac{\sigma_\eta^2}{1-a^2}\, a^{|m|}.$$

Taking the Fourier transform of $R_{xx}(m)$, one finds that

$$S_{xx}(\omega) = \sum_{m=-\infty}^{\infty} \frac{\sigma_\eta^2}{1-a^2} a^{|m|} e^{-j\omega m} = \frac{\sigma_\eta^2}{1+a^2-2a\cos\omega}, \quad -\pi \le \omega \le \pi.$$

An alternative way of obtaining $S_{xx}$ is to take the Fourier transform of both sides of Eq. (4.11) to obtain

$$X(\omega) = ae^{-j\omega}X(\omega) + \sigma_\eta, \tag{4.12}$$

where $X(\omega)$ denotes the Fourier transform of the left-hand side of Eq. (4.11), and the coefficient $e^{-j\omega}$ on the right-hand side of Eq. (4.12) is due to delay by one unit of time. It is easy to see that

$$S_{xx}(\omega) = |X(\omega)|^2.$$

We thus verify the Wiener-Khintchine theorem.

### 4.1.3 Sampling theorem

Suppose we sample a CT signal $x(t)$ to obtain a DT signal $x(n)$ with a fixed time interval $T$. The inverse of $T$ is called the sampling frequency, $F_s = 1/T$. Based on

$$t = nT = n/F_s,$$

what relation can be derived between the Fourier transform $X(f)$ of $x(n)$ and the Fourier transform $X_a(F)$ of $x(t)$? It is

$$X(f) = X\left(\frac{F}{F_s}\right) = F_s \sum_{k=-\infty}^{\infty} X_a(F - kF_s). \tag{4.13}$$

The right-hand side of Eq. (4.13) consists of a periodic repetition of the scaled spectrum $F_s X_a(F)$ with period $F_s$. This periodicity is necessary, since $X(f)$ is periodic with period 1. When the repeating copies of $F_s X_a(F)$ do not overlap, we

say that the sampling frequency is high enough that no aliasing has occurred. This is ensured when $X_a(F)$ is band-limited to the interval $(-F_s/2, F_s/2)$. Formally, the sampling theorem can be stated that a band-limited CT signal, with highest frequency (bandwidth) $B$ Hz, can be uniquely recovered from its samples provided that the sampling rate $F_s$ is at least $2B$ samples per second.

### 4.1.4 Discrete Fourier transform

The discrete Fourier transform (DFT) and its inverse (IDFT) are defined by

$$\text{DFT}: \quad X(k) = \sum_{n=0}^{N-1} x(n)e^{-j2\pi kn/N} \quad k = 0, 1, 2, \cdots, N-1 \quad (4.14)$$

$$\text{IDFT}: \quad x(n) = \frac{1}{N} \sum_{k=0}^{N-1} X(k)e^{j2\pi kn/N} \quad n = 0, 1, 2, \cdots, N-1. \quad (4.15)$$

The derivations of DFT and IDFT involve periodic extension of the signal sequence $x(n)$, $n = 0, 1, \cdots, N-1$. Therefore, one can expect Eq. (4.14) to be similar to Eq. (4.6) , while Eq. (4.15) is similar to Eq. (4.5). This is indeed the case. In fact, the difference is only by the factor $1/N$. This difference is by convention. It is not essential.

DFT has a number of interesting properties. We note one here. It indicates that for a real signal, $|X(k)|$ is symmetric about $N/2$. This is because

$$X(N-k) = X^*(k), \quad (4.16)$$

where the superscript * denotes a complex conjugate. Therefore, for a real signal, it is sufficient to plot out the magnitude and phase of $X(k)$ for $k = 0, 1, \cdots, N/2$, since $X(k)$ for $k = N/2+1, \cdots, N-1$ does not contain any new information. This property can also be considered an action of the sampling theorem.

### 4.1.5 Fourier analysis of real data

To truly understand Fourier analysis, it is essential to have hands-on experience with real data. We analyze four types of data here: parkinsonian tremor, quantum well device noise, DNA sequence, and EEG.

**Example 1**: A tremor is an involuntary, approximately rhythmic, and roughly sinusoidal movement of parts of the body. Broadly speaking, there are two classes of tremors: normal and pathologic. Pathologic tremors result from disorders of the central and peripheral nervous systems. The two most common ones are the essential tremor (ET) and the tremor in Parkinson's disease (PD). In PD, a typical 4–6 Hz resting tremor is observed, whereas in ET, the rhythmic activation of the muscles typically occurs at a higher frequency: 5–10 Hz. Figure 4.1(a) shows a signal of a parkinsonian tremor. The data were sampled at a rate of 1000 Hz. Figure 4.1(b) shows the PSD of the data.

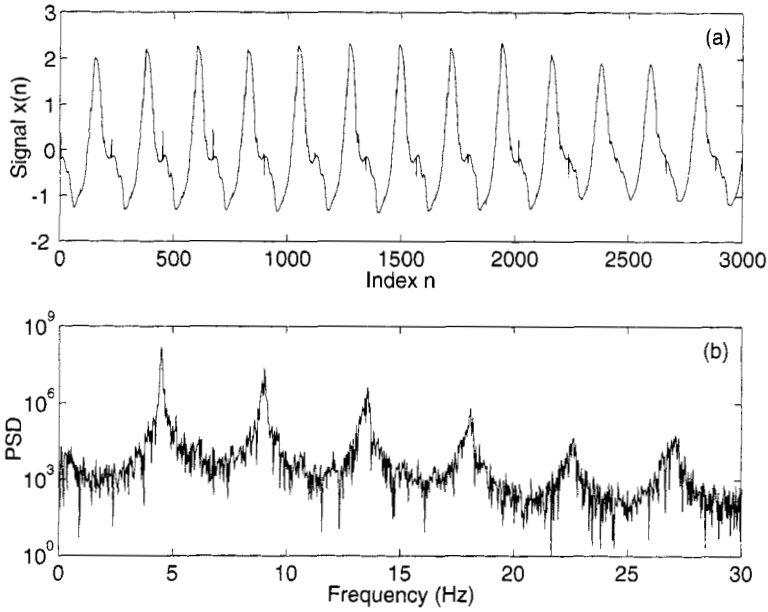


**Figure 4.1.** Parkinsonian tremor signal (a) and its PSD (b).

We now make a few comments.

1. In real data analysis, it is more useful to specify the unit for the frequency axis than to use the normalized frequency. This can be done as follows. Given a sequence of $N$ points, sampled at a sampling rate of $F_s$, the total time interval monitored is $N/F_s$. The frequency $f_k$ corresponding to the $k$th point $X(k)$ is

$$f_k = \frac{k}{N} F_s.$$

In particular, $X_0$ is called the DC component, contributed by the mean of the signal. In situations where the DC component is much stronger than other frequency components, it is desirable to remove the DC component before taking the Fourier transform (or equivalently, set $X_0 = 0$).

2. When $T_s = 1/F_s = 1$ unit and the signal is known to have a period $T_i$, one may expect to observe a sharp spectral peak at

$$i = \frac{N}{T_i}.$$

This feature will be made clearer when we discuss the period-3 feature in coding the DNA sequence in example 3.

3. In the digital signal processing class of one of the authors, J.B., many students plotted the spectrum for the entire frequency range $0 \leq f \leq 1000$ Hz. Then only

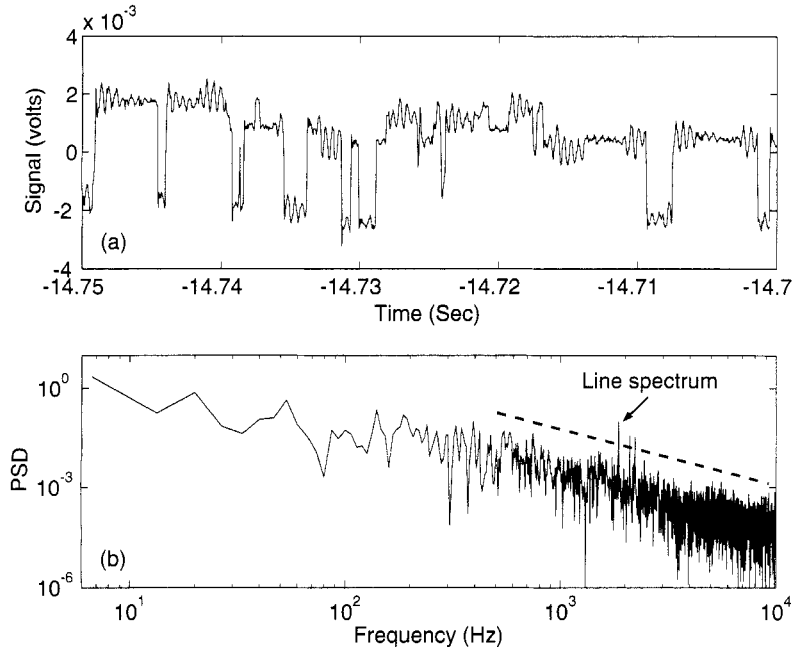


**Figure 4.2.** (a) Noise recorded in a quantum well infrared photodetector; (b) the PSD of the noise.

nonzero spectrum could be seen along the two ends. After being reminded that at least the right half of the spectrum does not need to be plotted, many students plotted the spectrum for $0 \leq f \leq 500$ Hz. Still, not much could be seen. This example emphasizes that one needs to zoom in and out to find out which frequency band is significant.

4. In the so-called Bode plots, the frequency axis is plotted logarithmically. When Fig. 4.1(b) is plotted in log scale, the spacing between successive harmonics is no longer of equal distance. This hinders visual inspection. Therefore, the linear scale for the frequency axis is more appropriate for observing harmonics.

**Example 2**: We now discuss noise recorded in a quantum well infrared photodetector, with a sampling time of 50 $\mu s$. Figure 4.2(a) shows a segment of the noise trace. It is like an ON/OFF train. In the literature, such noise is called a random telegraph signal (RTS). Its PSD is shown in Fig. 4.2(b), where we observe that the PSD decays in a power-law manner. This is an example of so-called $1/f^{\beta}$ noise, a special type of random fractals. The dashed straight line shown in Fig. 4.2(b) has a slope approximately equal to $-1$. Therefore, $\beta \approx 1$ here. To more accurately estimate the $\beta$ parameter, we must use methods to be discussed in Chapter 8.

Again, we make two comments.

1. Why is it important to study a spectrum of the $1/f^{\beta}$ shape? The reason is that a power-law decaying spectrum is a well-defined functional form, and therefore

warrants a physical explanation of how it is generated. The most popular model in the study of device noise (including this as well as the more general MOSFET noise) is the relaxation model. This model relates the spectrum to the distribution of the ON/OFF periods of the RTS. This will be explained in more detail in Chapter 11.

2. Figure 4.2(b) contains a few spectral lines indicated by an arrow. In J.B.'s digital signal processing class, some students thought that those lines correspond to the true signal, while the rest of the spectrum is due to noise. This is not correct. In fact, the spectral lines are not important at all. They are the noise from the measurement equipment.

**Example 3**: A DNA sequence is made up of four nucleotides: adenine (A), guanine (G), thymine (T), and cytosine (C). A and G are purines, while T and C are pyrimidines. A DNA sequence is highly complicated, containing many functional structures. On the coarsest level, a DNA sequence can be partitioned into alternating coding and noncoding segments. The coding region has a salient feature of period-3 (P3), resulting from the fact that three nucleotide bases encode an amino acid and that the usage of codons is highly biased. This P3 feature can be readily manifested by the Fourier transform. Specifically, one can map a DNA sequence of length $N$ to a numerical sequence (for example, C and T to 1, A and G to $-1$), and then take the Fourier transform. One can then observe a strong peak at or around $N/3$. See Fig. 4.3(a). Usually, such a strong peak cannot be observed in noncoding regions, as shown in Fig. 4.3(b).

Another main feature of a DNA sequence is its randomness. It is not like simple white noise. One good way of analyzing its randomness is to form the so-called DNA walk,

$$y(n) = \sum_{k=0}^{n} u(k),$$

where $u(k)$ is the numerical sequence mapped from the DNA sequence. An example is shown in Fig. 4.4. The PSD of a DNA walk is also of the form $1/f^{\beta}$, similar to that shown in Fig. 4.2(b). It has been found that $\beta$ is close to 2 for coding sequences but may differ from 2 quite significantly for noncoding sequences. Again, estimation of $\beta$ using Fourier analysis may not be accurate enough. More accurate methods will be developed in Chapter 8. We should nevertheless emphasize that this does not mean that Fourier analysis is useless for analyzing fractal signals. In fact, qualitative understanding using Fourier analysis can serve as a guide in the further refined analysis.

**Example 4**: Brain waves (EEGs) result from electrical activity emanating from the brain. The signals can be highly nonstationary, as shown in Fig. 4.5(a). There are four categories of brain waves. Ranging from most to least active, they are beta, alpha, theta, and delta waves. The beta wave is associated with the brain's being aroused and actively engaged in mental activities. The alpha wave represents the nonarousal state of the brain. The theta wave is associated with drowsiness/idling,

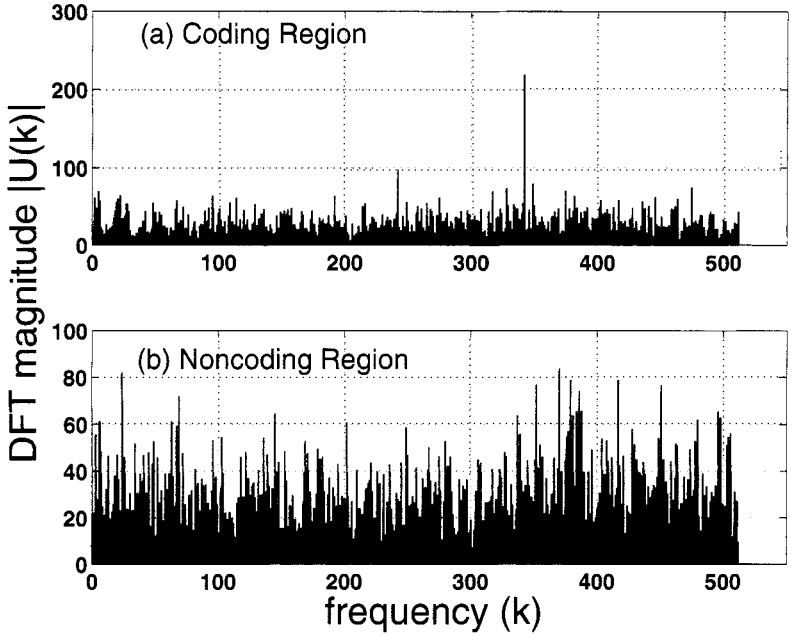


**Figure 4.3.** Representative DFT magnitude for coding and noncoding regions in yeast chromosome I.

and the delta wave is associated with sleep/dreaming. The exact frequency ranges for the four waves may vary among researchers, however. For example, one Internet document states that the four waves correspond to frequency ranges $14-40$, $7.5-13$, $3.5-7.5$, and $< 3$ Hz (i.e., cycles per second), respectively. Another document states that they correspond to $15-40$, $9-14$, $5-8$, and $1.5-4$ Hz. Other research papers may give slightly different values.

One, especially a layman, could ask whether the four waves are characterized by distinct spectral peaks in the frequency domain. It turns out that they are not. One example is shown in Fig. 4.5(b) for a fairly stationary EEG segment. We do not observe any distinct spectral speaks. In Chapter 15, we shall discuss the physical meaning of these waves.

## 4.2 WAVELET MULTIRESOLUTION ANALYSIS

In situations where the time dependence of the frequency of a given signal is of interest, one could resort to windowed Fourier transformations (WFT). However, WFT is not always an effective solution, since sharp localizations in time and in frequency cannot be simultaneously achieved. The wavelet transform solves this problem by utilizing the scaled and shifted versions of a wavelet, $\psi(t)$, using the

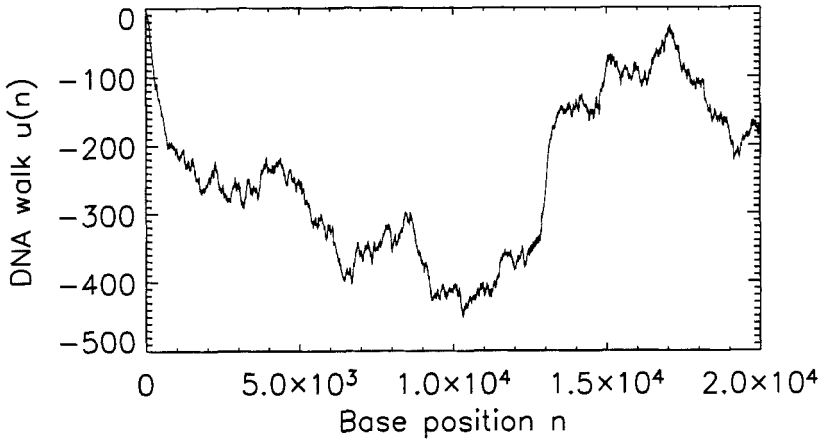


**Figure 4.4.** An example of a DNA walk constructed from the first 20,000 bases of the chromosome I of yeast.

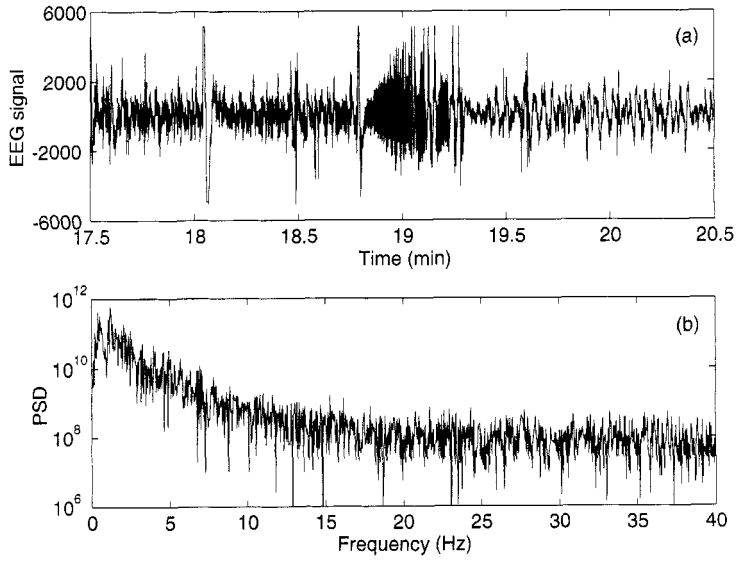


**Figure 4.5.** (a) A segment of EEG signal; (b) its PSD.

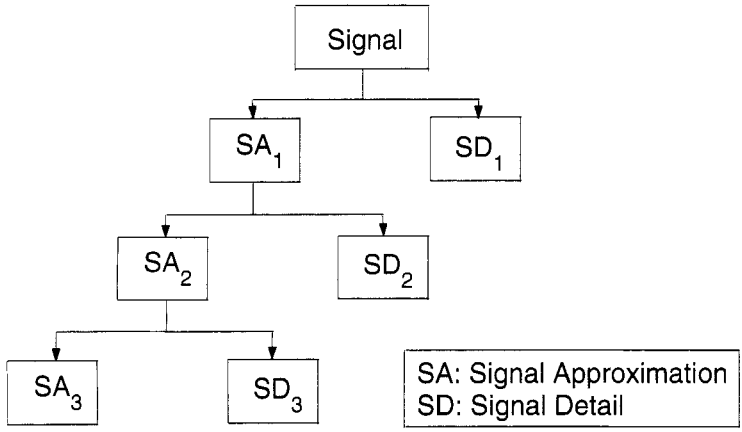


**Figure 4.6.** Pyramidal structure of the output of wavelet MRA.

following equation:

$$\psi_{s,k}(t) \equiv \psi_s(t-k) = |s|^{-p}\psi\Big(\frac{t-k}{s}\Big),$$

where $p > 0$ is fixed, $k$ is the translation, and $s$ is the scale. The translation or shifting achieves time localization of the signal, while the use of scale $s$ avoids commitment to any particular scale. To see the latter, let us take $k = 0$. Then, when $s > 1$, $\psi_s(t)$ is the version of $\psi$ stretched by the factor $s$ in the horizontal direction; when $0 < s < 1$, $\psi_s$ is a compressed version of $\psi$. When $s < 0$, $\psi_s(t)$ is not only stretched or compressed but also reflected. Wavelet transform is concerned with expressing a function in terms of $\psi_{s,k}(t)$ for all $(s, k)$.

Around 1986, a very powerful method, multiresolution analysis (MRA), for performing discrete wavelet analysis and synthesis was developed. This is a recursive method. One begins with a version $x^0 = \{x(n)\}$ of the signal sampled at regular time intervals $\Delta t = \tau > 0$. The signal $x^0$ is split into a "blurred" version $SA_1$ at the coarser scale $\Delta t = 2\tau$ and "detail" $SD_1$ at scale $\Delta t = \tau$. This process is repeated, giving a sequence $x^0$, $SA_1$, $SA_2, \cdots$ of more and more blurred versions together with the details $SD_1$, $SD_2, SD_3, \cdots$, where the scale for $SA_m$ is $2^m\tau$, while the scale for $SD_m$ is $2^{m-1}\tau$. The function $SA_j$, $j > 0$ is also called approximation of the original signal at resolution level $j$. After $J$ iterations, the original signal is reconstructed as

$$x^0 = SA_J + SD_1 + SD_2 + \cdots + SD_J.$$

This is schematically shown by the pyramidal structure in Fig. 4.6.

More precisely, MRA involves an iterative application of the scaling function $\phi_0$ and the wavelet function $\psi_0$. The scaling function is a low-pass filter. It satisfies the condition

$$\int_{-\infty}^{\infty} \phi_0(t)dt = 1.$$

The wavelet $\psi_0$ must have zero average and decay quickly at both ends. It is a high-pass filter. The scaled and shifted versions of $\phi_0$ and $\psi_0$ are given by

$$\phi_{j,k}(t) = 2^{-j/2}\phi_0(2^{-j}t - k),$$
$$\psi_{j,k}(t) = 2^{-j/2}\psi_0(2^{-j}t - k),$$

where $j, k \in Z$ are the scaling (dilation) index and the shifting (translation) index, respectively. Different values of $j$ correspond to analyzing different resolution levels of the signal. With the scaling function and the mother wavelet, MRA can be described by the following steps:

1. At the $j = 1$th resolution, for each $k = 0, 1, 2, \cdots$, compute the approximation coefficient $a_x(j,k)$ and the detailed coefficient $d_x(j,k)$ according to the following formula:

$$a_x(j,k) = \sum_n x(n)\phi_{j,k}(n) = \sum_n x(n)2^{-j/2}\phi_0(2^{-j}n - k), \quad (4.17)$$
$$d_x(j,k) = \sum_n x(n)\psi_{j,k}(n) = \sum_n x(n)2^{-j/2}\psi_0(2^{-j}n - k). \quad (4.18)$$

2. The signal approximation $SA_j$ and the signal detail $SD_j$ at the $j$th resolution level are computed as

$$SA_j = \sum_k a_x(j,k)\phi_{j,k}(n), \quad (4.19)$$
$$SD_j = \sum_k d_x(j,k)\psi_{j,k}(n). \quad (4.20)$$

   Note that the resolution for $SA_1$ and $SD_1$ is $2\tau$ and $\tau$, respectively.

3. Repeat steps 1 and 2 for the $(j+1)$th resolution level, using the signal approximation $SA_j$ obtained in step 2 as the input signal. Note that the resolution for $SD_{j+1}$ is the same as that for $SA_j$, which is $2^j\tau$, while the resolution for $SA_{j+1}$ is $2^{j+1}\tau$, twice as coarse as that for $SA_j$.

Let the maximum scale resolution level chosen for analysis be $J$. The reconstruction formula is

$$x(n) = SA_J + \sum_{j=1}^{J} SD_j = \sum_k a_x(J,k)\phi_{J,k}(n) + \sum_{j=1}^{J}\sum_k d_x(j,k)\psi_{j,k}(n). \quad (4.21)$$

The first term represents the approximation at resolution level $J$, and the second term represents the details at resolution level $J$ and lower.

To make the above procedure more concrete, let us take the Haar wavelet as an example. The scaling function and the mother wavelet of the Haar wavelet are defined as

$$\phi_0(t) = \begin{cases} 1, & 0 \le t < 1, \\ 0 & \text{elsewhere.} \end{cases}$$

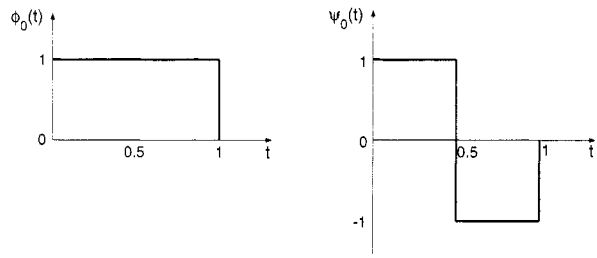


**Figure 4.7.** The scaling function $\phi_0(t)$ and the mother wavelet $\psi_0(t)$ of the Haar wavelet.

$$\psi_0(t) = \begin{cases} 1, & 0 \le t < 1/2, \\ -1, & 1/2 \le t < 1, \\ 0 & \text{elsewhere.} \end{cases}$$

They are depicted in Fig. 4.7.

To understand how the Haar wavelet works, let us compute a few terms of $a_x(j,k)$ and $d_x(j,k)$ according to Eqs. (4.17) and (4.18). When $j = 1,\ k = 0$, we have

$$a_x(1,0) = 2^{-1/2}[x(1) + x(2)], \quad \text{simple smoothing}$$

$$d_x(1,0) = 2^{-1/2}[x(1) - x(2)], \quad \text{simple differencing.}$$

When $j = 1,\ k = 1$, we have

$$a_x(1,1) = 2^{-1/2}[x(3) + x(4)], \quad \text{simple smoothing}$$

$$d_x(1,1) = 2^{-1/2}[x(3) - x(4)], \quad \text{simple differencing.}$$

At the next resolution level $j = 2$, when $k = 0$, we have

$$a_x(2,0) = 2^{-1}[x(1) + x(2) + x(3) + x(4)] = 2^{-1/2}[a_x(1,0) + a_x(1,1)],$$

$$d_x(2,0) = 2^{-1}[x(1) + x(2) - x(3) - x(4)] = 2^{-1/2}[a_x(1,0) - a_x(1,1)].$$

Evidently, $\phi_0(t)$ is a low-pass filter, while $\psi_0(t)$ is a high-pass filter. For the Haar wavelet, for each resolution level $j$, the maximal $k$ is $2^{-j}N$, where $N$ is the length of the dataset. For wavelets with more complicated functional forms for $\phi_0(t)$ and $\psi_0(t)$, Eqs. (4.17) and (4.18) amount to smoothing and differencing with weights given by shifting and compressing/dilating $\phi_0(t)$ and $\psi_0(t)$, respectively.

We now further illustrate the Haar wavelet by analyzing an example signal $x(n)$, which consists of noisy blocks, as shown in Fig. 4.8(a). The signal approximations and details at resolution levels 1 through 3 are shown in Figs. 4.8(b,d,f) (left column) and Fig. 4.8(c,e,g) (right column), respectively. We have

$$x(n) = SA_1 + SD_1 = SA_2 + SD_2 + SD_1 = SA_3 + SD_3 + SD_2 + SD_1.$$

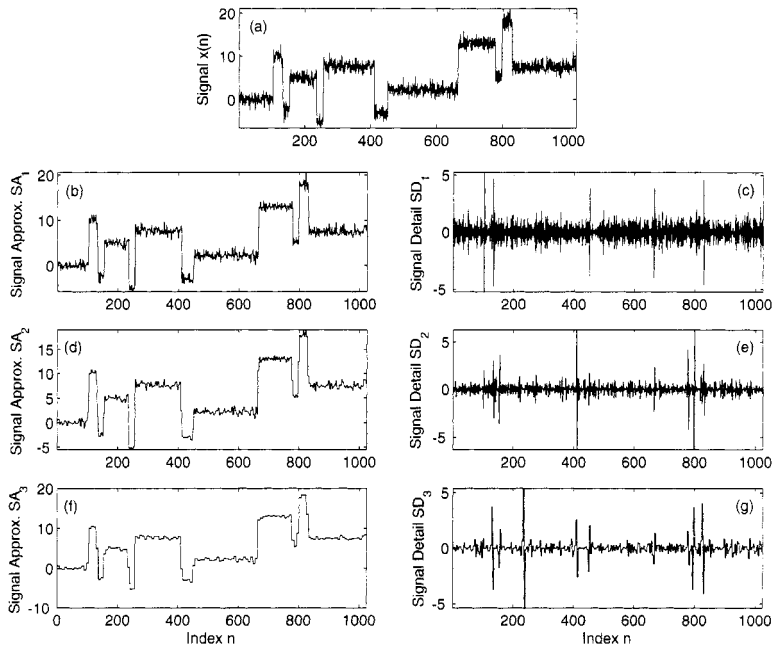


**Figure 4.8.** (a) The input signal $x(n)$, (b,d,f) and (c,e,g) are the signal approximations and the signal details at resolution levels 1 through 3, respectively. $x(n) = SA_1 + SD_1 = SA_2 + SD_2 + SD_1 = SA_3 + SD_3 + SD_2 + SD_1$.

## 4.3 BIBLIOGRAPHIC NOTES

Fourier analysis is a central topic in numerous excellent textbooks on signal processing. We refer to [324, 355, 413] here. For wavelet MRA, we refer to [414]. For more information about tremor data, we refer to [150, 175, 435]; about quantum well noise data, we refer to [271]; about DNA sequence data, we refer to [154, 159]; and about EEG data, we refer to [61, 176].

## 4.4 EXERCISES

1. Prove the Parsavel's relation described by Eq. (4.7).
2. Prove the symmetric property of DFT given by Eq. (4.16).
3. Continuing with the example of the Haar wavelet, write expressions for the approximation and detailed coefficients at the level $j = 3$.
4. Using the data downloadable at the book's website (see Sec. A.4 in Appendix A), re-produce Figs. 4.1, 4.2, and 4.5. There are many other datasets at this website. You may want to take a look at some of them.